electronics

MDPI

Article

Progress on Second-Generation High-Temperature Superconductor Tape Targeting Resistive Fault Current Limiter Application

Jiamin Zhu [1,2,*], Sikan Chen [2] and Zhijian Jin [1,*]

[1] School of Electronic Information and Electrical Engineering, Shanghai Jiao Tong University, Shanghai 200240, China
[2] Shanghai Superconductor Technology Co., Ltd., Shanghai 201203, China; sikan.chen@shsctec.com
* Correspondence: jiamin.zhu@shsctec.com (J.Z.); zjjin@sjtu.edu.cn (Z.J.)

Abstract: The resistive superconducting fault current limiter is well known for its simple structure and outstanding current-limiting effect, and it is broadly applied in power grid systems. The second-generation high-temperature superconductor (HTS) tape, of higher structural strength and greater room-temperature resistance, is well suited for application in resistive superconducting fault current limiters. The quenching caused by overcurrent in the HTS tape is a complexed coupling effect of several physical factors. The tape structure and properties directly impact the ultimate HTS tape's quench performance. In this study, various SS316-laminated HTS tapes, of different critical currents, room-temperature resistances, and masses, were prepared. The pulse impact parameters of the various tape samples were measured using the RLC high-current impact test platform. By analyzing the resultant data, a quantitative assessment methodology to measure a tape's tolerance toward impact was developed. The dependence of the HTS tape's tolerance toward impact on its critical current, room-temperature resistance, and mass was studied. This provides numerical guidance on HTS material selection for resistive superconducting fault current limiters.

Keywords: resistive superconducting fault current limiter; HTS tape; lamination; resistance to pulse impact; resistance response

Citation: Zhu, J.; Chen, S.; Jin, Z. Progress on Second-Generation High-Temperature Superconductor Tape Targeting Resistive Fault Current Limiter Application. *Electronics* **2022**, *11*, 297. https://doi.org/10.3390/electronics11030297

Academic Editor: Davide Brunelli

Received: 16 December 2021
Accepted: 14 January 2022
Published: 18 January 2022

1. Introduction

As power systems increase in capacity and complexity, large short-circuit fault current is one of the main factors threatening the safety and stability of power systems. It is, thus, critical to effectively limit short-circuit fault currents in power systems. Considering the limitations of high-capacity circuit breaker, a superconducting current limiter is a good alternative [1–5].

There are two types of superconducting current limiters: saturated iron core current limiter and resistive current limiter. As the second-generation HTS tapes enter the commercialization stage, more and more enterprises can mass-produce the second-generation HTS tapes [6–13]. Compared with the first-generation tapes, 70% of which were made from silver, the second-generation tapes have higher structural strength, greater room-temperature resistance, and higher quench recovery speed, which has attracted research interest to be applied for resistive current limiters [14].

A resistive superconducting fault current limiter (R-SFCL) is a device that operates on the state transition characteristics of superconductors. Its working principle and structure are simple, and its current-limiting effect is outstanding. At present, R-SFCL has been studied in many countries in the world, and many prototypes have been produced and tested in different power systems [15]. AMSC (Boston, MA, USA), and Siemens (France), developed the first 115 kV/1.2 kA transformer R-SFCL [16,17]. KEPCO (South Korea), developed a 154 kV RSFCL [18,19]. SuperOx (Russia), developed a 220 kV/1.2 kA current

limiter [20]. Shanghai Jiaotong University (China), developed a 10 kV/200 A current limiter [21,22]. Using the HTS tapes supplied by Shanghai Superconductor Technology Co., Ltd. (SST), (China), Zhongtian Technology (China), developed a 220 kV/1.5 kA resistive current limiter [23], and Guangdong Power Grid (China), jointly developed a ±160 kV/1.0 kA resistive current limiter [24].

Extensive studies have been carried out on testing HTS tapes for resistive fault current limiter application. Llambes et al. [25] and Hajdasz et al. [26] studied the application of superpower tapes in SFCL; Schmidt et al. [27] and Baldan et al. [28,29] studied the application of AMSC tapes in SFCL; Ahn et al. [30], Park et al. [31], and Sheng et al. [32] compared the tape structures from different postprocessing treatments in the application of SFCL; Lacroix et al. [33,34] developed a novel structure to increase the NZPV (normal zone propagation velocity) of HTS tape during impulse impact; Zhang et al. [35] and Liu et al. [36] determined the DC overcurrent impact on the tapes at different temperatures and analyzed quench resistance; Sheng et al. [37] and Maeda et al. [38] studied the quench recovery of the tapes after overcurrent impact and observed the bubbles generated by heat transfer on the tape surface during the quench process; Xiang et al. [39] studied the effect of magnetic field on the overcurrent impact of tapes; Rusiński et al. [40] and Jiang et al. [41] studied the effect of tape insulation on overcurrent impact; Liang et al. [42,43] modeled the quench resistance of the tape through the R–Q curve; LV et al. [44] laminated the optical fiber on the side of the tape to measure the temperature during the overcurrent impact process.

Most of the prior studies were based upon mature commercialized HTS tapes. By optimizing tape structure to improve the relevant parameters, the performance of fault current limiters can be further improved. From previous studies, it was evident that, given the same room-temperature resistance, laminated tapes were 2–3 times better in terms of overcurrent impact resistance than copper-plated tapes. In this paper, the preparation process of SST tapes for resistive fault current limiters is elaborated in detail. By means of calculation, experiment, and photography, the effects of metal layer constituents on the impact tolerance and characteristics of stainless-steel laminated HTS tapes are studied. This provides a basis for the selection of tapes for resistive superconducting current limiters.

2. Experimental Details

2.1. Preparation of Samples

The YBCO superconducting tapes used in the experiments were produced by SST [39]. $Al_2O_3/Y_2O_3/MgO/LaMnO_3/CeO_2$/REBCO/Ag layers were successively plated on 50 μm thick 10 mm wide Hastelloy^{TM} substrate. Depending on the requirements of actual application, copper electroplating and lamination can be added to the tapes. The resistive superconducting fault current limiter requires the tapes to have high room-temperature resistance and high impact tolerance. Previous studies have shown that stainless-steel laminated tape has better performance than copper-plated tape in these aspects; hence, stainless steel was chosen to encapsulate the tapes.

Figure 1 shows the basic structure of an HTS tape used in a fault current limiter. This is the actual structure of the samples studied in this paper. The metal layers of the tape primarily included a silver stabilizing layer, copper stabilizing layer, stainless-steel reinforcing layer, and tin solder layer. The silver layer was plated by magnetron sputtering. In order to ensure full protection of the superconducting layer and save cost, the side on the superconducting surface was plated with 1.5 μm, the side on the Hastelloy^{TM} surface was plated with 0.5 μm. Electrochemical copper plating was applied outside the silver layer. The wettability of the silver layer and tin solder was rather poor, but the wettability of copper and tin solder was good. In order to keep the layers bonded together, copper plating is an essential step. To prevent it from melting and being scratched in the lamination process, the copper plating layer needs to maintain a minimum thickness of 2 μm per side. Whether silver or copper is plated, the sides of the tapes need to be plated to form an integral coverage. Lamination primarily uses the welding method ("sandwich" type

encapsulation) to adhere two layers of encapsulation on the upper and lower sides of the superconducting tape. The solder composition used in the experiments was Pb63Sn37. The width of the stainless-steel lamination tape was 12 mm, and 1 mm wide gaps on both sides were filled with solder to ensure that the encapsulated superconducting tape formed a complete cladding structure. In addition, the interlayers between stainless-steel tape and superconducting tape are filled with solder, and the external surfaces of stainless steel were also covered with solder. The thickness of the interlayer and coated solder was about 4 µm.

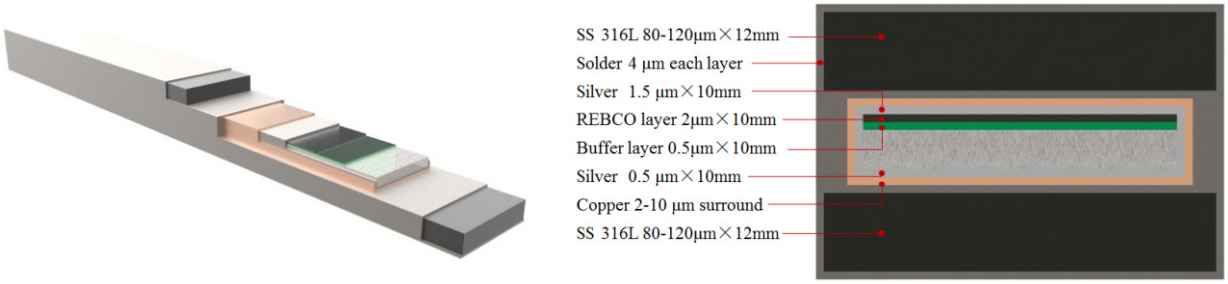

Figure 1. (**a**) Cross-section of laminated tape used for SFCL; (**b**) cross-sectional area of each material.

When not in a superconducting state, the superconductor layer and the buffer layers are considered as oxide materials, with electrical resistance much higher than metals. Hence, their resistances were excluded in resistance calculation. The resistance of every metal layer can be calculated using the formula below.

$$R = \rho_R \frac{L}{S} \tag{1}$$

where L is the length of metal, S is the cross-sectional area, and the ρ_R of individual metals at various temperatures can be found in Table 1.

Table 1. Material parameters.

Material	Density (kg/m^3)	Specific Heat J/(kg·K)		Resistivity $\times 10^{-8}$ Ω·m	
		77 K	295 K	77 K	295 K
Silver (Ag)	1.05×10^4	187	236	0.27	1.60
Copper (Cu)	8.93×10^3	254	386	0.23	1.73
Hastelloy (Has)	8.89×10^3	251	427	124.00	127.00
SS 316L (Sus)	7.98×10^3	251	490	56.80	77.10
Solder 63/37 (Sn)	8.78×10^3	155	182	3.00	15.00

From the structure of the laminated HTS tape, it is assumed that there is no current transfer among the metal layers; the variation of resistance of the above-described metal layers with temperature T can be calculated using the following formula as conductors in parallel:

$$\frac{1}{R_{SC}(T)} = \frac{1}{R_{Has}(T)} + \frac{1}{R_{Ag}(T)} + \frac{1}{R_{Cu}(T)} + \frac{1}{R_{Sus}(T)} + \frac{1}{R_{Sn}(T)}. \tag{2}$$

Upon eliminating certain items from the above equation, the room-temperature resistance of products from individual processing steps can be calculated and, thus, controlled. For example, the HTS tape product after silver plating has a resistance of

$$\frac{1}{R_{SCAg}(T)} = \frac{1}{R_{Has}(T)} + \frac{1}{R_{Ag}(T)}. \tag{3}$$

Transport measurements on a large amount of Hastelloy^{TM} substrates, of 50 μm thickness and 10 mm width, allowed concluding that its room-temperature resistance is around 2700 mΩ/m. After applying the buffer layers and superconductor layer, the room-temperature resistance remained approximately the same. The HTS tape after silver plating measured about 610 mΩ/m.

The mass of each metal layer can be calculated using density as shown below.

$$m = \rho_D V = \rho_D LS, \tag{4}$$

where L is the length of metal, S is the cross-sectional area, and the ρ_R of individual metals at various temperatures can be found in Table 1.

Hence, the sum of all metal layers is

$$m_{Sc} = (\rho_{Has}S_{Has} + \rho_{Ag}S_{Ag} + \rho_{Cu}S_{Cu} + \rho_{Sus}S_{Sus} + \rho_{Sn}S_{Sn})L, \tag{5}$$

where ρ_{Has} is the density of Hastelloy^{TM}, ρ_{Ag} is the density of the silver layer, ρ_{Cu} is the density of the copper layer, ρ_{Sus} is the density of the stainless-steel layer, ρ_{Sn} is the density of the tin solder.

In the calculation, the contribution of buffer layer and superconducting layer oxides to the resistance and specific heat capacity of HTS tape was ignored. In the temperature range of 77 K–400 K, it is assumed that the resistivity and specific heat capacity of the metal layers change linearly with temperature. As a result, the curves of resistance and specific heat capacity against temperature, of a specific HTS tape, can be obtained by calculation.

For a resistive superconducting fault current limiter, the critical current, room-temperature resistance, and impact tolerance of HTS tape are important parameters, which directly determine the performance indices of the fault current limiter. In order to study the effects of metal layer composites in the stainless-steel laminated HTS tape on its impact tolerance, 12 laminated tapes of various specifications were prepared, as shown in Table 2.

Samples 1–4 used 80 + 80 μm stainless steel for lamination, while the room-temperature resistance of the tapes was kept constant at 100 mΩ/m, Tc of the superconductor layer was 92 K, and critical currents of the tapes were varied with different HTS layer thickness. Sample 1 had no superconductor layer, but its other layers were identical to other samples. Samples 4–8 were laminated with 80 + 80 μm stainless steel, while the critical current of the tapes was kept at 500 A, and the room-temperature resistance of the tapes was varied to 100, 90, 80, 70, and 60 mΩ/m. For samples 4 and 9–12, the room-temperature resistance of the tapes was kept at 100 mΩ/m and the critical current was kept at 500 A, while the thickness of the stainless-steel lamination layers of the tapes was varied to 80 μm, 100 μm, and 120 μm.

The room-temperature resistance variation in samples was realized by adjusting the thickness of the copper layer. It emerged from the sample preparation process that it was extremely difficult to accurately control the room-temperature resistance of the tapes. This is because, although the volume and mass content of silver and copper in the HTS tape were very low, their resistivity was much lower than that of other materials, and the resistance of silver and copper layers also varied greatly with temperature, which had a significant impact on the total resistance of HTS tape. It can be seen from the calculated value of copper plating thickness in Table 2 that the thickness of copper plating was very low and required very precise control. A thickness difference of 0.1 μm could bring about a significant change in room temperature resistance.

Table 2. Specimen ID and corresponding specifications.

	Nominal I_C	Actual I_C	Cu Thickness Calculated Value	Lamination Thickness	Nominal Resistance at RT	Actual Resistance at RT	Mass, Calculated Value	Mass, Actual Value
Sample 1	0 A	0 A	3.29 μm	(80 + 80) μm	100 mΩ/m	101.0 mΩ/m	22.6 g/m	22.6 g/m
Sample 2	100 A	101 A	3.50 μm	(80 + 80) μm	100 mΩ/m	98.5 mΩ/m	22.7 g/m	22.9 g/m
Sample 3	300 A	288 A	3.41 μm	(80 + 80) μm	100 mΩ/m	99.6 mΩ/m	22.6 g/m	22.9 g/m
Sample 4	500 A	510 A	3.38 μm	(80 + 80) μm	100 mΩ/m	100.0 mΩ/m	22.6 g/m	22.6 g/m
Sample 5	500 A	501 A	4.34 μm	(80 + 80) μm	90 mΩ/m	89.8 mΩ/m	22.8 g/m	22.7 g/m
Sample 6	500 A	502 A	5.45 μm	(80 + 80) μm	80 mΩ/m	80.2 mΩ/m	23.1 g/m	22.9 g/m
Sample 7	500 A	500 A	6.97 μm	(80 + 80) μm	70 mΩ/m	70.0 mΩ/m	23.4 g/m	23.2 g/m
Sample 8	500 A	498 A	9.51 μm	(80 + 80) μm	60 mΩ/m	58.1 mΩ/m	23.8 g/m	24.1 g/m
Sample 9	500 A	506 A	2.96 μm	(80 + 100) μm	100 mΩ/m	101.9 mΩ/m	24.5 g/m	24.3 g/m
Sample 10	500 A	511 A	2.78 μm	(100 + 100) μm	100 mΩ/m	101.1 mΩ/m	26.3 g/m	26.0 g/m
Sample 11	500 A	510 A	2.47 μm	(100 + 120) μm	100 mΩ/m	101.1 mΩ/m	28.6 g/m	28.2 g/m
Sample 12	500 A	510 A	2.45 μm	(120 + 120) μm	100 mΩ/m	98.1 mΩ/m	30.5 g/m	30.7 g/m

From Table 2, it can be concluded that the mass per unit length of tape calculated using Equation (5) was rather consistent with the mass obtained by actual weighing.

2.2. Test Platform

To assess the transient overcurrent characteristics of HTS tape, the high-current impulse test platform was used as shown in Figure 2. The energy storage discharge mode of the capacitor was used to generate DC single pulses to simulate the impact of DC power grid short-circuit fault current on the HTS tapes.

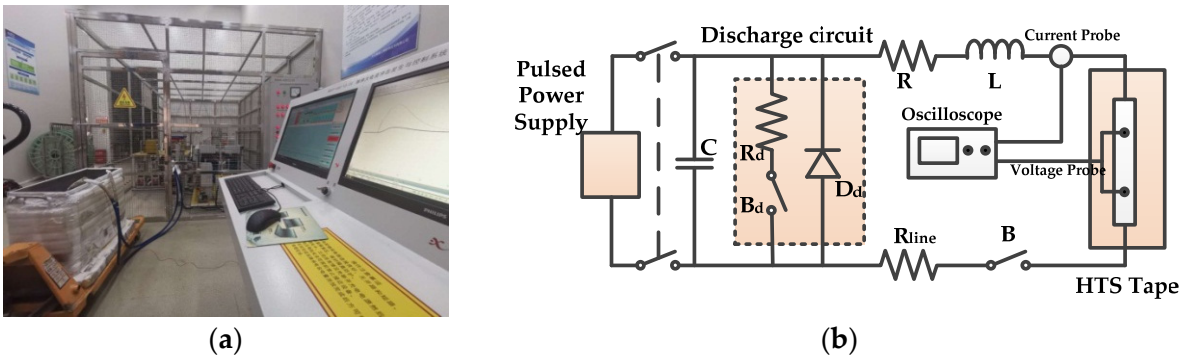

(**a**) (**b**)

Figure 2. (**a**) Transient current experiment platform; (**b**) circuit diagram.

Before the test, the capacitor was charged at different energy levels by varying the capacitor charging voltages. The impulse pulse width was controlled by setting the inductance and resistance. The data acquisition part of the system was achieved using a high-precision oscilloscope, current transformer, and voltage probe. The capacitor output was steadily increased by increasing its voltage setting stepwise, and the impact test was carried out on the tapes until they were burned in the system short-circuit, in order to study the overcurrent impact tolerance of the HTS tapes.

The circuit was an RLC series circuit composed of resistor, inductor, and capacitor. It was a zero-input response process of a second-order circuit. A second-order homogeneous differential equation with constant coefficients where u_c is unknown could, thus, be formulated.

$$LC\frac{d^2u_c}{dt^2} + RC\frac{du_c}{dt} + u_c = 0, \tag{6}$$

or

$$\frac{d^2u_c}{dt^2} + \frac{R}{L}\frac{du_c}{dt} + \frac{1}{LC}u_c = 0. \tag{7}$$

The characteristic equation is

$$s^2 + \frac{R}{L}s + \frac{1}{LC} = 0. \tag{8}$$

Solving the differential equations gives

$$s_{1,2} = -\frac{R}{2L} \pm \sqrt{\left(\frac{R}{2L}\right)^2 - \frac{1}{LC}}. \tag{9}$$

When $> 2\sqrt{\frac{L}{C}}$, it is an over-damped condition, and its solution is

$$u_c(t) = K_1e^{s_1t} + K_2e^{s_2t}, \tag{10}$$

$$i_L(t) = C\frac{du_c}{dt}. \tag{11}$$

When $R = 2\sqrt{\frac{L}{C}}$, it is a critically damped condition, and its solution is

$$i_c(t) = K_1 e^{s_1 t} + K_2 e^{s_2 t}. \tag{12}$$

When $< 2\sqrt{\frac{L}{C}}$, it is an under-damped condition, and its solution is

$$u_c(t) = e^{-at}[K_1 cos(\omega_d t) + K_2 sin(\omega_d t)], \tag{13}$$

$$i_L(t) = C\frac{du_c}{dt}. \tag{14}$$

Substituting in initial conditions gives the actual solutions.

Ignoring the resistance of superconducting tape and the circuit, the capacitance was 8 mF, and the resistance R and inductance L in the circuit were adjustable parameters. The charging voltage of the capacitor was fixed at 1 kV, and the impact test was carried out on sample 4.

L was set to 0.2 mH, and R was changed to obtain different current, voltage, and resistance response waveforms, as shown in Figure 3. It can be seen that the increasing sides of the current were basically identical, and the decreasing sides became gentler with resistance increase.

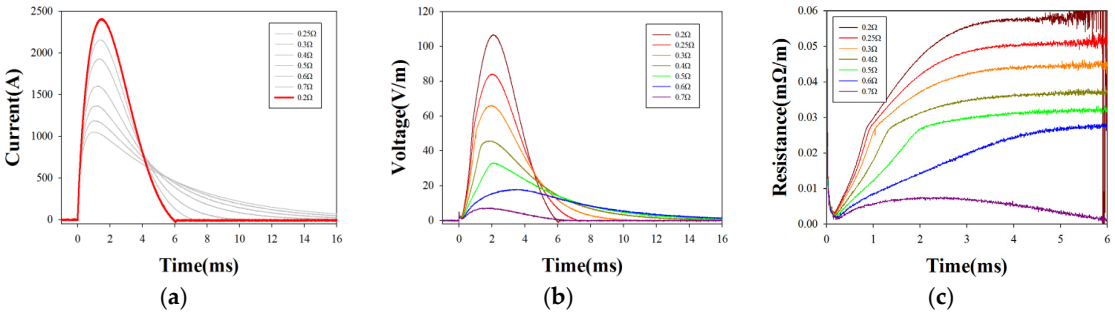

Figure 3. Fixed impulse test platform L = 0.2 mH while varying R: (**a**) impulse current waveform; (**b**) impulse voltage waveform; (**c**) resistance response waveform.

R was set to 0.2 mΩ, and L was changed to obtain different current, voltage, and resistance response waveforms, as shown in Figure 4. It can be seen that the current waveform increased and decreased more or less symmetrically. As inductance increased, the duration of overcurrent impact impulse increased.

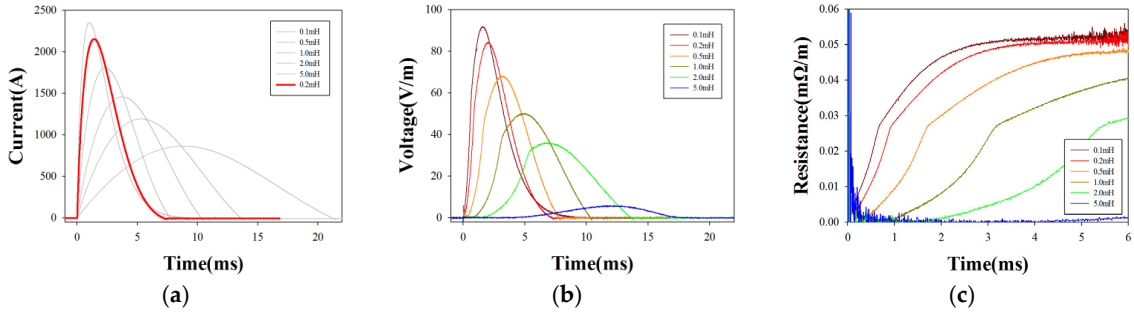

Figure 4. Fixed impulse test platform with R = 0.2 mΩ while varying L: (**a**) impulse current waveform; (**b**) impulse voltage waveform; (**c**) resistance response waveform.

Some differences can also be observed in the impulse voltage curve and resistance response curve. At present, superconducting current limiters mainly focus on the response performance within 5 ms of short-circuit current; therefore, the system setting parameters

of R = 0.2 mΩ and L = 0.2 mH were finally selected to conduct impact tests on the HTS tapes, as shown by the red lines in Figures 3a and 4a.

3. Results and Discussion

3.1. Experimental Results and Analysis for Typical Samples

Individual samples were subjected to impact, and the corresponding impulse current and impulse voltage waveforms were obtained. The distance between the voltage taps on the tape was 8 cm. Figure 5 shows the waveform of sample 4. For better visualization, the voltage was converted to volt per meter.

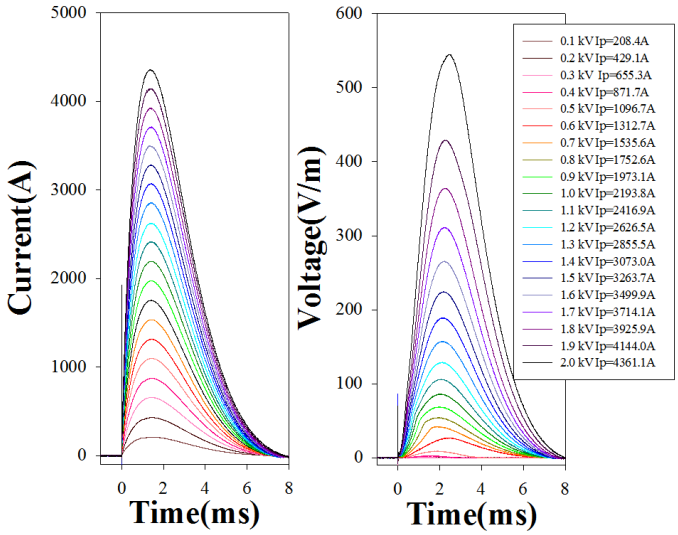

Figure 5. Transient impulse current and voltage waveform of sample 4.

The curve of Figure 6 was obtained by calculation using data from Figure 5. Under the impact of large current, the resistance increased rapidly. Since the metal resistance variation with temperature between 77 K and 600 K was rather linear, the temperature corresponding to the resistance of a sample could be identified, as marked on the right vertical axis of Figure 6. The red dotted line in the figure indicates the temperature of 456 K, which is the melting point of tin solder.

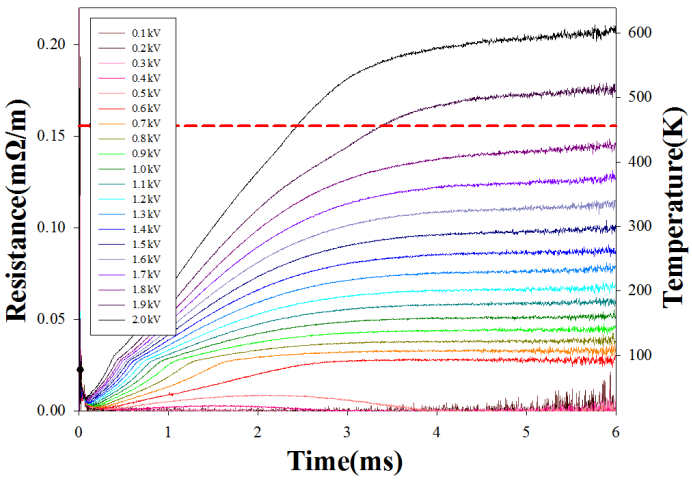

Figure 6. Transient resistance per meter of sample 4 under impact.

The appearance of the tape samples before impact tests is shown in Figure 7a. The samples were visually inspected after each impact test. When the tape was impacted normally, the surface was the same as that before impact. When the sample was impacted

with a 1.8 kV charged capacitor, the peak impulse current was 3925.9 A, and regional melting was observed on the surface of the HTS tape, as shown in Figure 7b. It can also be seen from Figure 6 that the temperature of the sample was close to the melting point temperature of the solder. When a 1.9 kV charged capacitor was used for impact, the peak impact current was 4144.0 A, and the strong impact force led to plastic deformation on the tape, while cracks appeared on the edge of the tape, as shown in Figure 7c. When a 2.0 kV charged capacitor was used for impact, the peak impact current was 4361.1 A, and the crack at the edge of the tape was further enlarged, while there were scorch marks on the surface of the tape, as shown in Figure 7d.

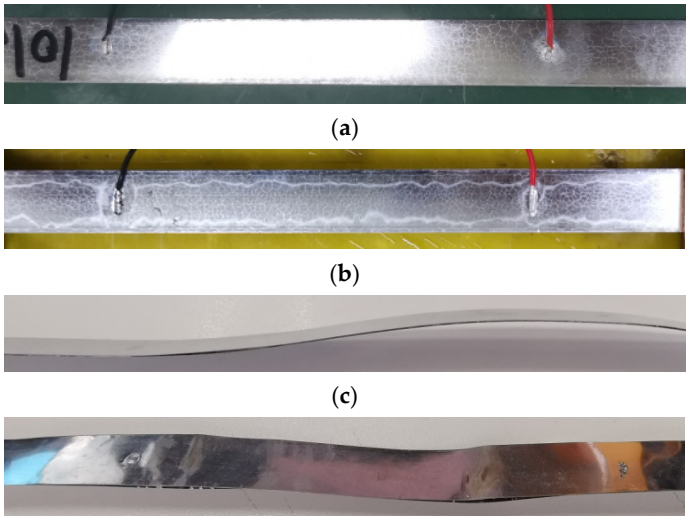

(**a**)

(**b**)

(**c**)

(**d**)

Figure 7. Surface conditions of sample 4: (**a**) before impact test; (**b**) when peak current was 3926.0 A; (**c**) when peak current was 4144.0 A; (**d**) when peak current was 4361.1 A.

The key factor influencing the temperature of the HTS tape should be the Joule heat generated during the quench process, which is determined by a combination of quench resistance, current, and quench time. The variation of Joule heat Q generated in the HTS tape with time can be calculated using Equation (15), and its unit is Joule (J).

$$Q_{heat} = \int_0^t I^2 R(t) dt, \tag{15}$$

where t is the quench time and $R(t)$ is the quench resistance corresponding to the quench time.

Figure 8 shows the variation of tape resistance per unit length with Joule heat following each impact of sample 4. Similar to Figure 6, the temperatures corresponding to the resistance of the sample were identified, as marked on the right vertical axis; the red dotted line in the figure indicates the melting point.

It can be seen from the figure that, with each increase in impact voltage, the increase in resistance became more rapid. The quench resistance response is a process of heat accumulation on the HTS tapes. The heat brought by impact leads to the increase in tape resistance, and the increase in resistance leads to additional heat generation. The accumulated heat of the tape itself can be expressed by the following equation:

$$Q_{accumulate} = \int_0^t c(T) m \frac{dT}{dt} dt. \tag{16}$$

Taking the cooling effect from liquid nitrogen into consideration, the following equations can be derived:

$$Q_{accumulate} = Q_{heat} - Q_{cool}, \tag{17}$$

$$Q_{accumulate}(t) = \int_0^t \left(I^2 R(t) - P_{cool} \right) dt. \tag{18}$$

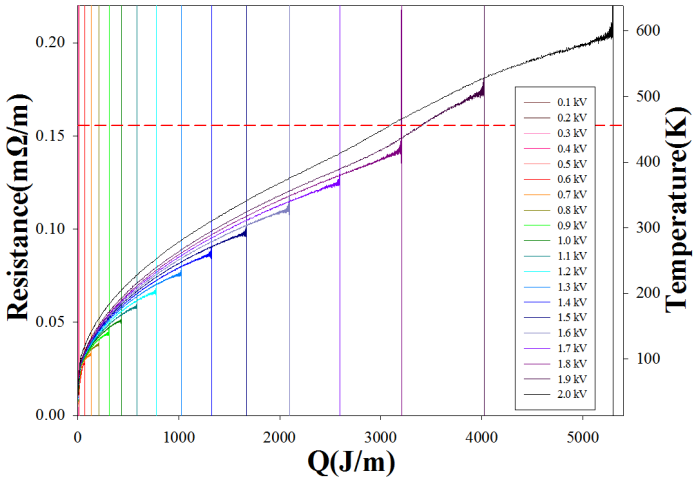

Figure 8. R–Q curves of sample 4 under impact.

In order to further investigate the problem, the R–Q curves of two impact tests were selected for analysis as shown in Figure 9. When impact was conducted with a 1.3 kV charged capacitor, the total heat generated by sample 4 in 7.28 ms was 1028.5 J. When impact was conducted with a 1.8 kV charged capacitor, the total heat generated by sample 4 in 1.72 ms was also 1028.5 J. However, the resistance response curves of the two were different at 76.2 mΩ/m and 87.1 mΩ/m, respectively. The temperatures achieved by the tapes were 230.5 K and 261.3 K, respectively, with a difference of 30.8 K. This temperature difference originated from the heat dissipation of liquid nitrogen with a time duration difference of 5.56 ms. It can be concluded that the different rates of resistance increase, manifested in Figure 8, resulted from the difference in heat dissipation by liquid nitrogen.

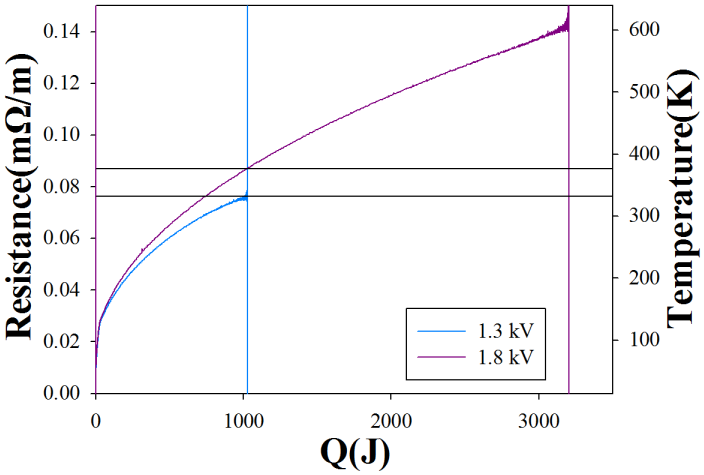

Figure 9. Typical R–Q curves of sample 4 under impact.

3.2. Comparison of Impact Tolerance

A comprehensive impact experiment was carried out on 12 samples using the overcurrent impact test platform. By examining the sample surfaces, the impact values leading to strictly no local surface melting were retained, and the corresponding peak current was identified, as listed in Table 3.

Table 3. Copper-plated and laminated HTS tape samples.

	Actual Resistance at RT	Calculated Resistance at 77 K	Actual Resistance at 77 K	Calculated Resistance at 456 K	Actual Resistance at 456 K	Peak Current During Impact	Heat Generated During Impact
Sample 1	101.0 mΩ/m	22.6 mΩ/m	24.5 mΩ/m	157.1 mΩ/m	156.0 mΩ/m	3687.2 A	3410 J
Sample 2	98.5 mΩ/m	21.7 mΩ/m	25.3 mΩ/m	153.6 mΩ/m	150.3 mΩ/m	3694.8 A	3440 J
Sample 3	99.6 mΩ/m	22.1 mΩ/m	25.0 mΩ/m	155.1 mΩ/m	156.4 mΩ/m	3694.0 A	3450 J
Sample 4	100.0 mΩ/m	22.2 mΩ/m	25.4 mΩ/m	155.6 mΩ/m	153.7 mΩ/m	3714.0 A	3410 J
Sample 5	89.8 mΩ/m	18.7 mΩ/m	21.9 mΩ/m	140.6 mΩ/m	139.7 mΩ/m	3923.1 A	3510 J
Sample 6	80.2 mΩ/m	15.9 mΩ/m	17.0 mΩ/m	126.2 mΩ/m	126.0 mΩ/m	4395.5 A	3540 J
Sample 7	70.0 mΩ/m	13.1 mΩ/m	14.0 mΩ/m	110.7 mΩ/m	110.6 mΩ/m	4849.9 A	3560 J
Sample 8	58.1 mΩ/m	10.1 mΩ/m	9.7 mΩ/m	92.4 mΩ/m	92.9 mΩ/m	5314.2 A	3570 J
Sample 9	101.9 mΩ/m	23.9 mΩ/m	28.0 mΩ/m	157.7 mΩ/m	152.5 mΩ/m	3741.7 A	3610 J
Sample 10	101.1 mΩ/m	24.6 mΩ/m	29.0 mΩ/m	155.7 mΩ/m	152.9 mΩ/m	4169.2 A	3960 J
Sample 11	101.1 mΩ/m	26.0 mΩ/m	29.6 mΩ/m	154.7 mΩ/m	153.6 mΩ/m	4372.6 A	4340 J
Sample 12	98.1 mΩ/m	25.8 mΩ/m	32.6 mΩ/m	150.0 mΩ/m	143.9 mΩ/m	4579.9 A	4650 J

Resistance of the 12 samples was measured using a transport current refrigeration and heating device in a closed environment. The resistance per unit length of the 12 samples at 77 K and 456 K was calculated by using the density and resistivity parameters of different metals in Table 1. It can be found that the two sets of values were rather close. The trend line deviations in the R–Q diagram and the resistance of the tapes at 456 K were used to jointly determine the heat generated during impact, as listed in Table 3.

3.2.1. Effect of Critical Current of the HTS Tapes

Samples 1–4 had the same structure and room-temperature resistances, while they varied only in the critical current *Ic*. As shown in Figure 10, the peak values of the overcurrent current I_{max} during HTS tape impact were about the same, and the anti-impact energy Q_{max} of all samples was also roughly identical. This shows that the impact tolerance to overcurrent is largely dependent on the structure of the HTS tapes and has little to do with the critical current of the tape itself.

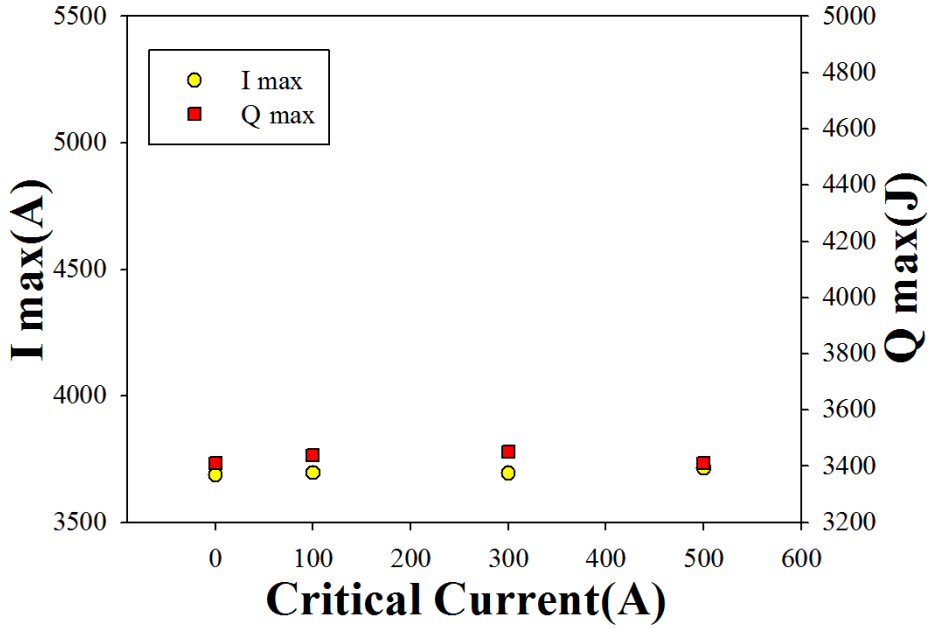

Figure 10. Impact tolerance performance of samples 1–4.

3.2.2. Effect of Room-Temperature Resistance of the HTS Tapes

For samples 4–8, the critical current of the HTS tapes was the same, and they were laminated with stainless steel of the same thickness. By slightly varying the thickness of copper plating, the room-temperature resistances of the tapes were manipulated to be 100, 90, 80, 70, and 60, respectively. As shown in Figure 11, as room-temperature resistance increased, the peak value of overcurrent impulse decreased. The overcurrent impact energy Q_{max} of the HTS tapes remained roughly constant. The amount of impact energy tolerated increased slightly as the thickness of the copper plating increased.

3.2.3. Effect of Mass of the HTS Tapes

For samples 4 and 9–12, the critical current of the HTS tapes was the same, and they were laminated with stainless steel of varying thickness. By slightly varying the thickness of copper plating, the room-temperature resistances of the tapes were controlled to be 100 m Ω/m. As shown in Figure 12, both the peak value of overcurrent impulse I_{max} and the overcurrent impact energy Q_{max} were positively correlated with the mass of the HTS tapes. This shows that higher mass provides a larger heat capacity, which is beneficial to withstand impact.

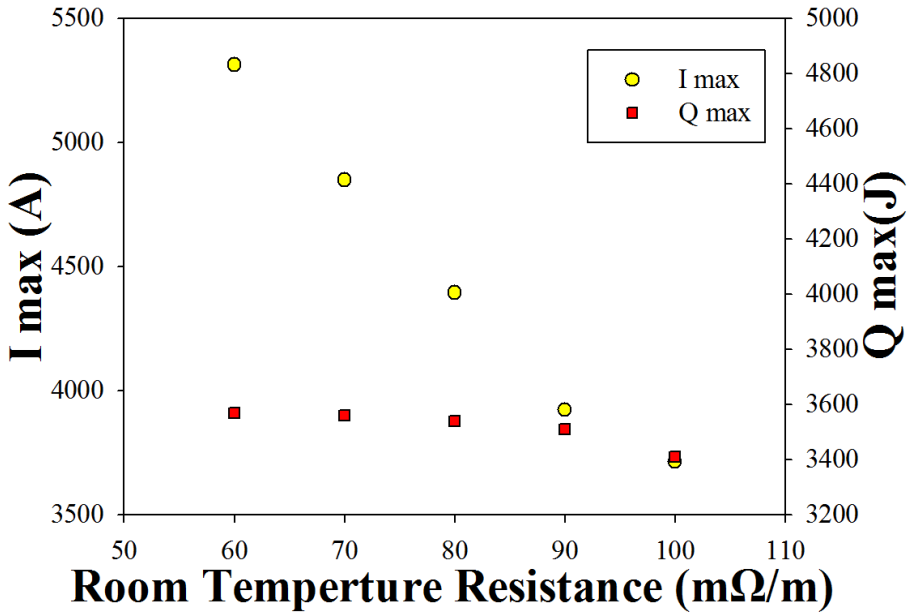

Figure 11. Impact tolerance performance of samples 4–8.

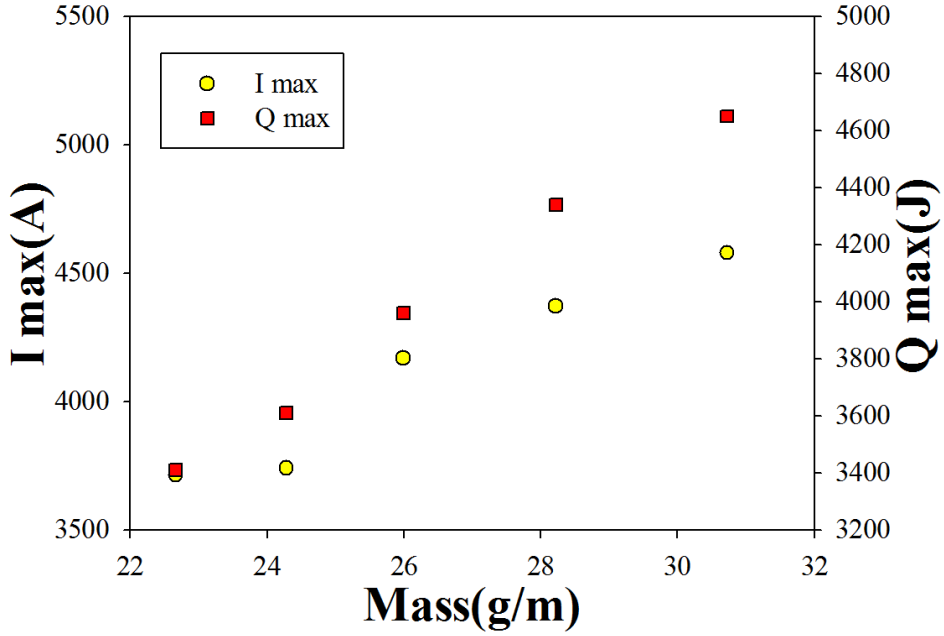

Figure 12. Impact tolerance performance of samples 4 and 9–12.

3.3. Resistance Response to Impulses

3.3.1. Impact of HTS Characteristics on Resistance Response to Impulses

In order to study the impulse resistance response of HTS tapes, a dummy sample with the same structure and resistance parameters as sample 4 was prepared. The only difference is that the dummy sample had no superconducting characteristics. Figure 13 shows the impulse current, impulse voltage, and corresponding resistance curves of the two samples under impacts of different energy level at 77 K.

Comparing Figure 13a,b, it can be seen that the impulse current curves of the two samples were basically the same. Comparing Figure 13c,d, it can be seen that the difference in impulse voltage between the two samples was only at the start. For the sample with zero *Ic*, the change in voltage was continuously conductive due to the lack of superconducting

characteristics. For the sample with *Ic* of 500 A, since the resistance at the beginning was 0, there was a process to enable quenching; hence, there was discontinuity in the first derivatives for parts of the curves, as shown by the red circles in Figure 13d, whereas the later parts of the curves were basically the same.

Figure 13e,f were calculated from the earlier graphs. It can be seen that the resistance of sample 1 and sample 4 was very different in the first 1 ms. The resistance of sample 1 increased from the unit resistance value of 22.60 mΩ/m at 77 K. In Figure 13e, this value is marked by a red dotted line. It can be seen that this basically coincided with the curve of impact at a low energy level. The resistance response curve of sample 4 showed a first-derivative discontinuity at 92 K, which is the critical temperature *Tc* of SST superconducting tape. In Figure 13f, this value is marked by a red dotted line. When the tape was impacted at different energy levels, the time taken to reach 92 K also varied.

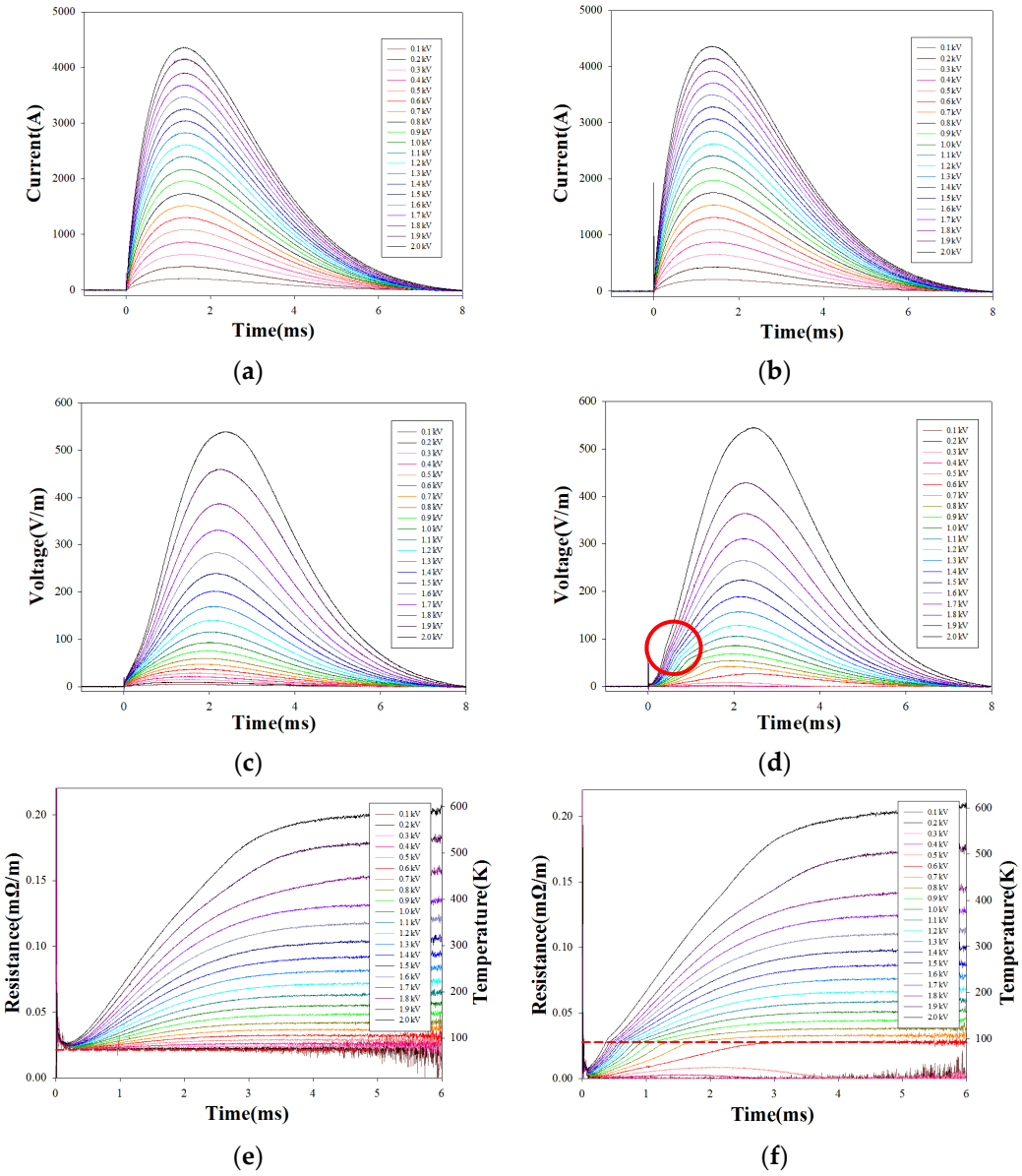

Figure 13. (**a**) Impulse current of sample 1; (**b**) impulse current of sample 4; (**c**) impulse voltage of sample 1; (**d**) impulse voltage of sample 4; (**e**) resistance response of sample 1; (**f**) resistance response of sample 4.

3.3.2. Impact of Critical Current on Resistance Response to Impulses

In order to further observe the effect of critical current on impulse resistance response, the impulse resistance curve of samples 1–4 was amplified and examined. It can be seen that the tape with *Ic* = 0 A was resistive in nature; therefore, when the 0.2 kV charged capacitor was used for impact, and the peak impulse current was 421.9 A, the impulse resistance was basically maintained at the 77 K resistance. With the further increase in impact energy, the impulse resistance response curve of the tape increased gradually.

For the tape with *Ic* =100 A, when the 0.5 kV charged capacitor was used for impact, the peak impulse current was 1081.7 A, which is the quenching threshold of the tape. When impacted at a lower energy level, even though the peak reached 863.9 A, the tape was only partially quenched. For tapes with *Ic* = 300 A and 500 A, the threshold of complete quench was reached. When the 0.6 kV charged capacitor was used for impact, the peak impulse current was about 1300 A. Comparing the different graphs in Figure 14, it can be seen that, after complete quench, the resistance response curves of tapes with different critical currents were similar; after partial quenches, the resistance response curves were rather different.

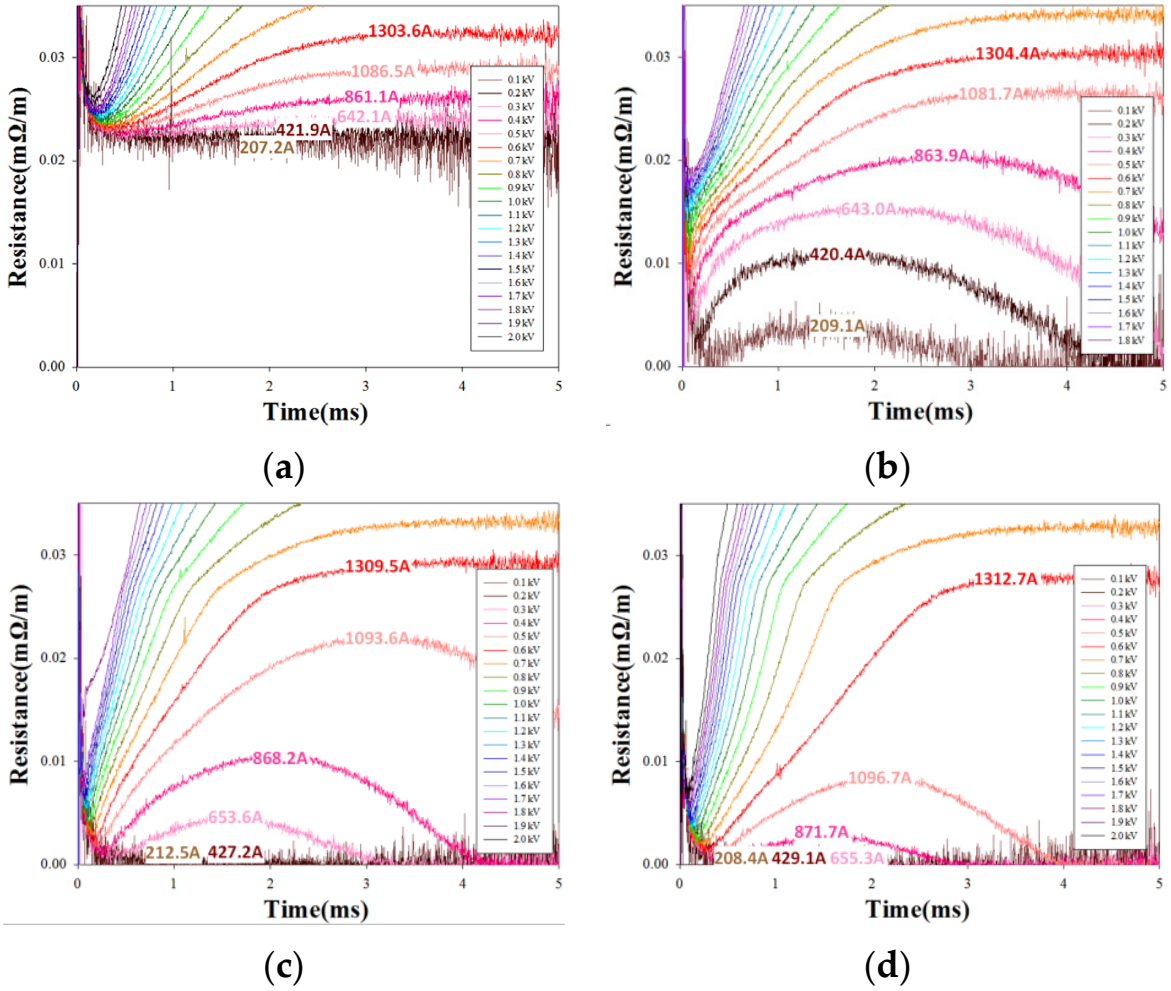

Figure 14. Impulse resistance responses of samples (**a**) sample 1; (**b**) sample 2; (**c**) sample 3; (**d**) sample 4.

Figure 15 compares the resistance response curves of samples 1–4 under the impact of 0.5 kV, 0.6 kV, 1.1 kV, and 1.7 kV capacitors. At 0.5 kV impact, the tapes were partially quenched, and the resistance response curves varied more evidently. At 0.6 kV impact, the tapes were completely quenched, the difference in resistance response curves decreased

after 3 ms, and a larger critical current led to lower quench resistance. At 1.1 kV and 1.7 kV impacts, the peak impulse current was about 2400 A and 3700 A, respectively. The quench resistances of HTS tapes were roughly identical.

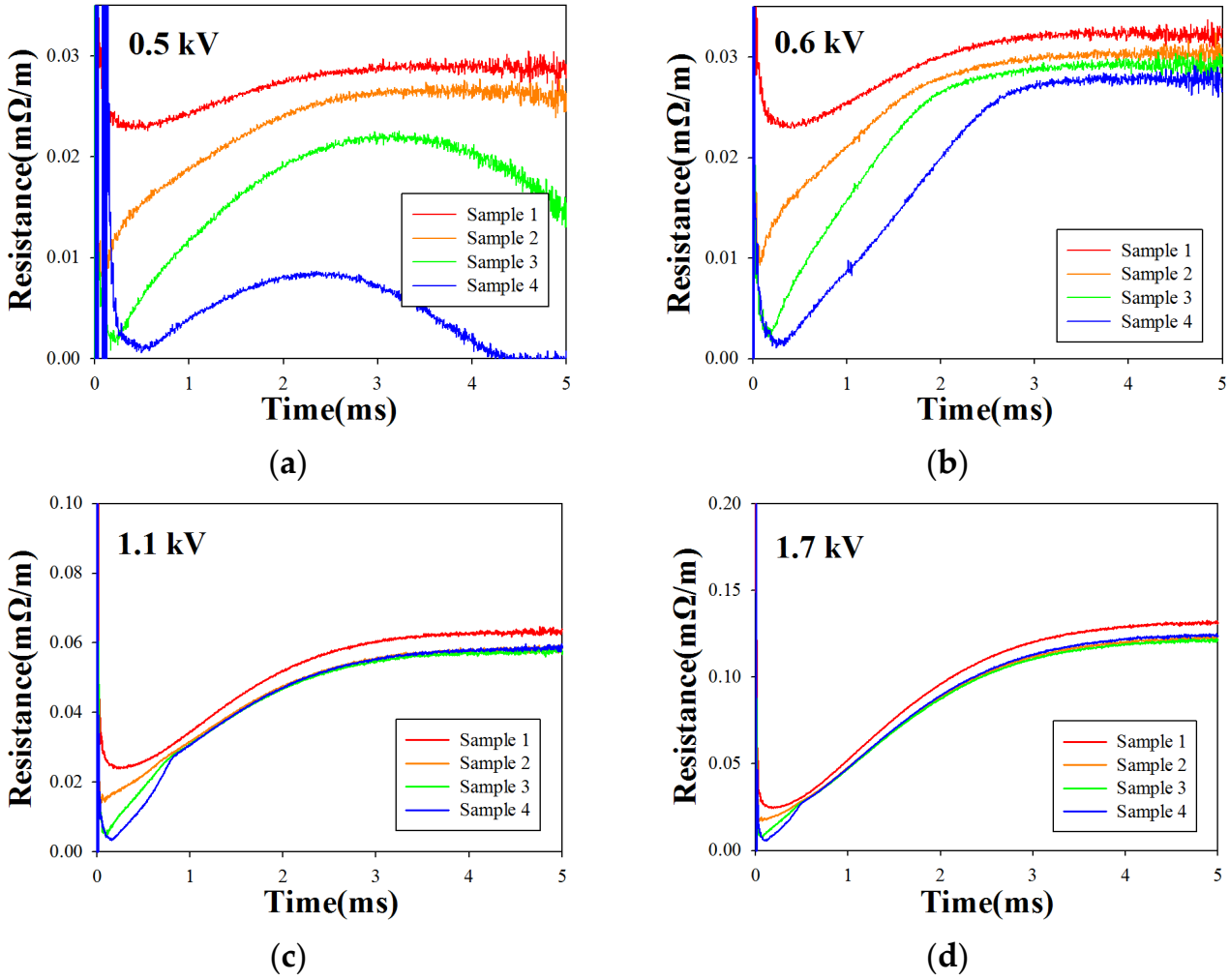

Figure 15. Impulse resistance response of samples 1–4: (**a**) 0.5 kV impact; (**b**) 0.6 kV impact; (**c**) 1.1 kV impact; (**d**) 1.7 kV impact.

3.3.3. Impact of Mass on Resistance Response to Impulses

Under the same overcurrent impact, the resistance response of HTS tapes with different room-temperature resistances varied significantly. From the study of samples 1–4, the resistance response of tapes with the same room-temperature resistance under the impact of equal overcurrent, especially under high-energy impact, had little difference. In order to more accurately study the impact performance of tapes with the same room-temperature resistance but different masses, samples 4, 10, and 12 were connected in series for the impact test, as shown in Figure 16, so as to ensure that the impact currents of the three were consistent.

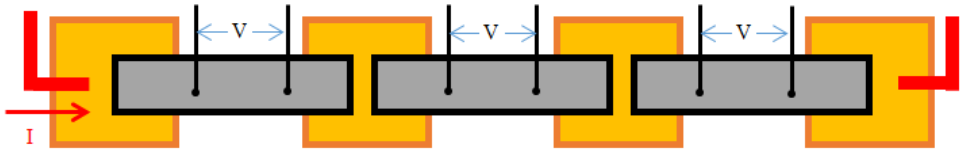

Figure 16. Schematic of samples 4, 10, and 12 in series for impact test.

As shown in Figure 17, when impacts were carried out with the capacitors charged at 0.5 and 0.6 kV, the quench resistance responses of the three samples were consistent. The quench of sample 4 was slightly slower than that of the other two samples because the sample resistance at 77 K was slightly lower. With a further increase in impact energy, the impact resistance response curve of the tape increased gradually. When the impact was carried out with the 1.1 kV charged capacitor, the quench resistance response of sample 4 began to surpass that of sample 10 and sample 12. When the impact was carried out with the 1.7 kV charged capacitor, the resistance responses of the three samples were significantly different. After 1 ms, the resistance of sample 4 was greater than that of sample 10 and sample 12. This shows that, for HTS tapes with the same room-temperature resistance, the tape of higher mass has a slower resistance response under impact.

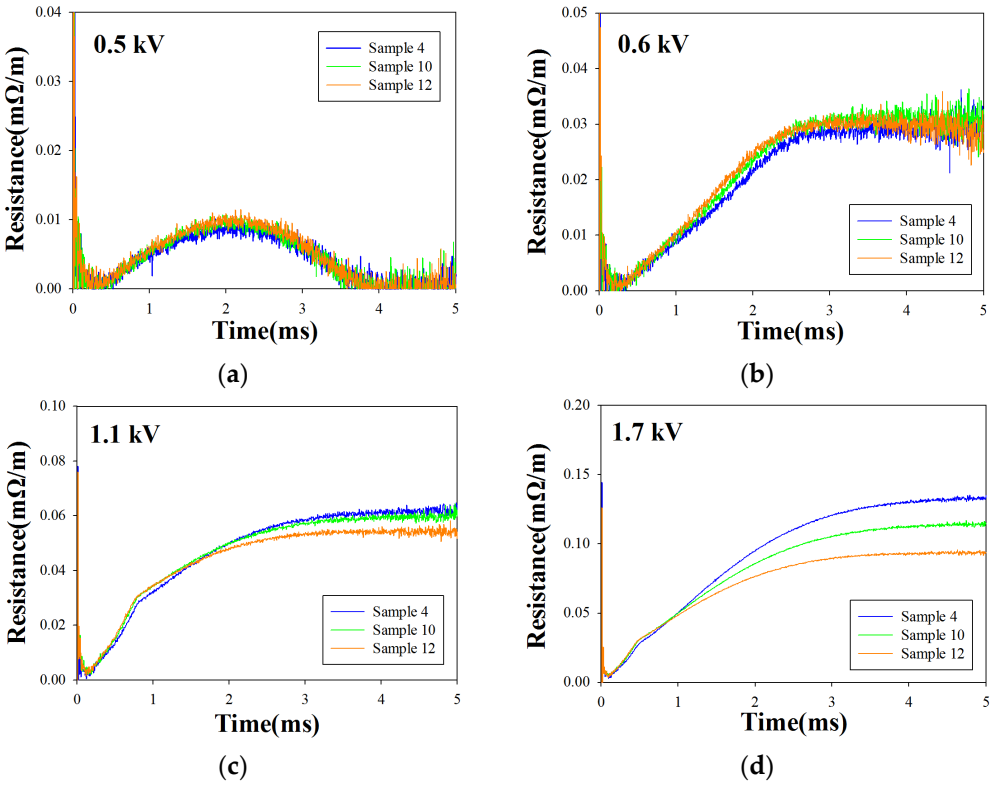

Figure 17. Impulse resistance response of samples 4, 10, and 12: (**a**) 0.5 kV impact; (**b**) 0.6 kV impact; (**c**) 1.1 kV impact; (**d**) 1.7 kV impact.

4. Conclusions

This paper mainly introduced the optimal design, quench characteristic assessment, and performance analysis of HTS tapes, as deployed in resistive current limiter applications. According to the HTS tape preparation and postprocessing techniques of Shanghai Superconducting Technology Co., Ltd., (China), HTS tape samples, targeting fault current limiter application, of variable mass per unit length, room-temperature resistance, critical current, and other key parameters, were prepared.

Working with 12 samples, through experiments and calculations, it was found that the quench performance of a tape in response to overcurrent is independent of its critical current, and it increases with the tape's thickness. When the overcurrent impact energy is maintained at a constant level, the peak value of overcurrent impulse is inversely related to the room-temperature resistance of a tape.

Following the quench behavior of HTS tape, there is a first-derivative discontinuity around Tc. When exposed to different levels of impact energy, the HTS tapes take different amounts of time to reach 92 K.

In this study, tapes of different critical current but the same structure demonstrated different impulse resistance responses below 1300 A impulse current. They started to demonstrate similar impulse resistance responses above 1300 A impulse current. As the degree of quench aggravated, at the same room-temperature resistance, a higher tape mass resulted in a slower resistance response under the same impact energy.

The design and assessment methodology for HTS tapes, described in this paper, could provide helpful guidance on material selection for resistive superconducting fault current limiters.

Author Contributions: Conceptualization, J.Z.; methodology, J.Z., S.C.; validation, J.Z.; formal analysis, J.Z., S.C.; investigation, J.Z., S.C.; resources, J.Z., Z.J.; data curation, J.Z.; writing—original draft preparation, J.Z.; writing—review and editing, J.Z.; visualization, J.Z., S.C.; supervision, Z.J.; project administration, J.Z.; funding acquisition, J.Z. All authors have read and agreed to the published version of the manuscript.

Funding: This research was funded by the Shanghai Rising-Star Program (Grant No. 20QB1401200) and the Scientific Research Program of the Science and Technology Commission of Shanghai Municipality (Grant No. 20511107500).

Acknowledgments: The authors would also like to acknowledge Tao Ma (Beijing Jiaotong University) and Jiangsu Zhongtian Technology Co. Ltd. for the help in setting up the transient current experiment platform.

Conflicts of Interest: The authors declare no conflict of interest.

References

1. Dommerque, R.; Krämer, S.; Hobl, A.; Böhm, R.; Bludau, M.; Bock, J.; Klaus, D.; Piereder, H.; Wilson, A.; Krüger, T.; et al. First commercial medium voltage superconducting fault-current limiters: Production, test and installation. *Supercond. Sci. Technol.* **2010**, *23*, 034020. [CrossRef]
2. Hobl, A.; Elschner, S.; Bock, J.; Kramer, S.; Janke, C.; Schramm, J. Superconducting fault current limiters: A new tool for the "grid of the future". In Proceedings of the CIRED 2012 Workshop: Integration of Renewables into the Distribution Grid, Lisbon, Portugal, 9–30 May 2012.
3. Stemmle, M.; Merschel, F.; Noe, M.; Hobl, A. AmpaCity—Advanced superconducting medium voltage system for urban area power supply. In Proceedings of the 2014 IEEE PES T&D Conference and Exposition, Chicago, IL, USA, 14–17 April 2014.
4. McGuckin, P.; Burt, G. Overview and assessment of superconducting technologies for power grid applications. In Proceedings of the 2018 53rd International Universities Power Engineering Conference (UPEC), Glasgow, UK, 4–7 September 2018.
5. Safaei, A.; Zolfaghari, M.; Gilvanejad, M.; Gharehpetian, G.B. A survey on fault current limiters: Development and technical aspects. *Int. J. Electr. Power Energy Syst.* **2020**, *118*, 105729. [CrossRef]
6. Rupich, M.W.; Li, X.; Sathyamurthy, S.; Thieme, C.L.; DeMoranville, K.; Gannon, J.; Fleshler, S. Second generation wire development at AMSC. *IEEE Trans. Appl. Supercond.* **2012**, *23*, 6601205. [CrossRef]
7. Selvamanickam, V.; Chen, Y.; Xiong, X.; Xie, Y.Y.; Reeves, J.L.; Zhang, X.; Qiao, Y.; Lenseth, K.P.; Schmidt, R.M.; Rar, A.; et al. Recent progress in second-generation HTS conductor scale-up at SuperPower. *IEEE Trans. Appl. Supercond.* **2007**, *17*, 3231–3234. [CrossRef]
8. Usoskin, A.; Betz, U.; Gnilsen, J.; Noll-Baumann, S.; Schlenga, K. Long-length YBCO coated conductors for ultra-high field applications: Gaining engineering current density via pulsed laser deposition/alternating beam-assisted deposition route. *Supercond. Sci. Technol.* **2019**, *32*, 094005. [CrossRef]
9. Stafford, B.H.; Sieger, M.; Ottolinger, R.; Meledin, A.; Strickland, N.M.; Wimbush, S.C.; Van Tendeloo, G.; Hühne, R.; Schultz, L. Tilted BaHfO3 nanorod artificial pinning centres in REBCO films on inclined substrate deposited-MgO coated conductor templates. *Supercond. Sci. Technol.* **2017**, *30*, 055002. [CrossRef]
10. Molodyk, A.; Samoilenkov, S.; Markelov, A.; Degtyarenko, P.; Lee, S.; Petrykin, V.; Gaifullin, M.; Mankevich, A.; Vavilov, A.; Sorbom, B.; et al. Development and large volume production of extremely high current density $YBa_2Cu_3O_7$ superconducting wires for fusion. *Sci. Rep.* **2021**, *11*, 2084. [CrossRef] [PubMed]
11. Fujita, S.; Muto, S.; Hirata, W.; Yoshida, T.; Kakimoto, K.; Iijima, Y.; Daibo, M.; Kiss, T.; Okada, T.; Awaji, S. Flux-pinning properties of BaHfO 3-doped EuBCO-coated conductors fabricated by hot-wall PLD. *IEEE Trans. Appl. Supercond.* **2019**, *29*, 8001505. [CrossRef]
12. Lee, J.H.; Lee, H.; Lee, J.W.; Choi, S.M.; Yoo, S.I.; Moon, S.H. RCE-DR, a novel process for coated conductor fabrication with high performance. *Supercond. Sci. Technol.* **2014**, *27*, 044018. [CrossRef]
13. Zhao, Y.; Zhu, J.M.; Jiang, G.Y.; Chen, C.S.; Wu, W.; Zhang, Z.W.; Chen, S.; Hong, Y.; Hong, Z.; Jin, A.; et al. Progress in fabrication of second generation high temperature superconducting tape at Shanghai Superconductor Technology. *Supercond. Sci. Technol.* **2019**, *32*, 044004. [CrossRef]

14. Bock, J.; Hobl, A.; Schramm, J.; Krämer, S.; Jänke, C. Resistive superconducting fault current limiters are becoming a mature technology. *IEEE Trans. Appl. Supercond.* **2014**, *25*, 5600604. [CrossRef]
15. Zhang, G.; Wang, H.; Qiu, Q.; Zhang, Z.; Xiao, L.; Lin, L. Recent progress of superconducting fault current limiter in China. *Supercond. Sci. Technol.* **2020**, *34*, 013001. [CrossRef]
16. Neumueller, H.W.; Schmidt, W.; Kraemer, H.P.; Otto, A.; Maguire, J.; Yuan, J.; Folts, D.; Romanosky, W.; Gamble, B.; Madura, D.; et al. Development of resistive fault current limiters based on YBCO coated conductors. *IEEE Trans. Appl. Supercond.* **2009**, *19*, 1950–1955. [CrossRef]
17. Kraemer, H.P.; Schmidt, W.; Cai, H.; Gamble, B.; Madura, D.; MacDonald, T.; McNamara, J.; Romanosky, W.; Snitchler, G.; Lallouet, N.; et al. Superconducting fault current limiter for transmission voltage. *Phys. Procedia* **2012**, *36*, 921–926. [CrossRef]
18. Lee, S.R.; Lee, J.J.; Yoon, J.; Kang, Y.W.; Hur, J. Protection scheme of a 154-kV SFCL test transmission line at the KEPCO power testing center. *IEEE Trans. Appl. Supercond.* **2017**, *27*, 5401305. [CrossRef]
19. Lee, S.R.; Ko, E.Y.; Lee, J.J.; Dinh, M.C. Development and HIL Testing of a Protection System for the Application of 154-kV SFCL in South Korea. *IEEE Trans. Appl. Supercond.* **2019**, *29*, 5401305. [CrossRef]
20. Moyzykh, M.; Gorbunova, D.; Ustyuzhanin, P.; Sotnikov, D.; Baburin, K.; Maklakov, A.; Magommedov, E.; Shumkov, A.; Telnova, A.; Shcherbakov, V.; et al. First Russian 220 kV superconducting fault current limiter (SFCL) for application in city grid. *IEEE Trans. Appl. Supercond.* **2021**, *31*, 5601707. [CrossRef]
21. Hong, Z.; Sheng, J.; Zhang, J.; Lin, B.; Ying, L.; Li, Y.; Jin, Z. The development and performance test of a 10 kV resistive type superconducting fault current limiter. *IEEE Trans. Appl. Supercond.* **2011**, *22*, 5600504. [CrossRef]
22. Chen, Y.; Liu, X.; Sheng, J.; Cai, L.; Jin, Z.; Gu, J.; An, Z.; Yang, X.; Hong, Z. Design and application of a superconducting fault current limiter in DC systems. *IEEE Trans. Appl. Supercond.* **2013**, *24*, 5601305. [CrossRef]
23. Dai, S.; Ma, T.; Xue, C.; Zhao, L.; Huang, Y.; Hu, L.; Wang, B.; Zhang, T.; Xu, X.; Cai, L.; et al. Development and test of a 220 kV/1.5 kA resistive type superconducting fault current limiter. *Phys. C Supercond. Its Appl.* **2019**, *565*, 1253501. [CrossRef]
24. Song, M.; Dai, S.; Sheng, C.; Zhong, L.; Duan, X.; Yan, G.; Huang, Y.; Chen, C.; Li, L.; Cai, L.; et al. Design and performance tests of a 160 kV/1.0 kA DC superconducting fault current limiter. *Phys. C Supercond. Its Appl.* **2021**, *585*, 1353871. [CrossRef]
25. Llambes, J.C.; Hazelton, D.; Duval, J.; Albertini, M.; Repnoy, S.; Selvamanickam, V.; Majkic, G.; Kesign, I.; Langston, J.; Steurer, M.; et al. Performance of 2G HTS tapes in sub-cooled LN2 for superconducting fault current limiting applications. *IEEE Trans. Appl. Supercond.* **2011**, *21*, 1206–1208. [CrossRef]
26. Hajdasz, S.; Kempski, A.; Rusinski, J. Study of HTS 2G superconductor tapes properties for applications in SFCL. In Proceedings of the 2018 Innovative Materials and Technologies in Electrical Engineering, Sulecin, Poland, 18–20 April 2018.
27. Schmidt, W.; Gamble, B.; Kraemer, H.P.; Madura, D.; Otto, A.; Romanosky, W. Design and test of current limiting modules using YBCO-coated conductors. *Supercond. Sci. Technol.* **2009**, *23*, 014024. [CrossRef]
28. Baldan, C.A.; Shigue, C.Y.; Lamas, J.S.; Ruppert Filho, E. Test results of a superconducting fault current limiter using YBCO coated conductor. *IEEE Trans. Appl. Supercond.* **2007**, *17*, 1903–1906. [CrossRef]
29. Baldan, C.A.; Lamas, J.S.; Shigue, C.Y.; Ruppert Filho, E. Fault current limiter using YBCO coated conductor—The limiting factor and its recovery time. *IEEE Trans. Appl. Supercond.* **2009**, *19*, 1810–1813. [CrossRef]
30. Ahn, M.C.; Yang, S.E.; Park, D.K.; Kang, H.; Seok, B.Y.; Ko, T.K. Current limiting characteristics of coated conductors with various stabilizers. *Cryogenics* **2007**, *47*, 425–430. [CrossRef]
31. Park, D.K.; Kim, M.J.; Yang, S.E.; Kim, Y.J.; Chang, K.S.; Na, J.B.; Ko, T.K. A study on the short circuit characteristic of metallic stabilizer free coated conductor for FCL application. *Prog. Supercond. Cryog.* **2007**, *9*, 37–40.
32. Sheng, J.; Zeng, W.; Ma, J.; Yao, Z.; Li, Z.; Jin, Z.; Hong, Z. Study of recovery characteristics of 2nd generation HTS tapes with different stabilizers for resistive type superconducting fault current limiters. *Phys. C Supercond. Its Appl.* **2016**, *521*, 33–37. [CrossRef]
33. Lacroix, C.; Sirois, F. Concept of a current flow diverter for accelerating the normal zone propagation velocity in 2G HTS coated conductors. *Supercond. Sci. Technol.* **2014**, *27*, 035003. [CrossRef]
34. Lacroix, C.; Lapierre, Y.; Coulombe, J.; Sirois, F. High normal zone propagation velocity in 2G HTS coated conductors with a current flow diverter architecture. *Supercond. Sci. Technol.* **2014**, *27*, 055013. [CrossRef]
35. Zhang, Z.; Yang, J.; Qiu, Q.; Zhang, G.; Lin, L. Research on resistance characteristics of YBCO tape under short-time DC large current impact. *Cryogenics* **2017**, *84*, 53–59. [CrossRef]
36. Liu, S.; Xia, D.; Qiu, Q.; Zhang, Z.; Wang, H.; Liu, Q. Threshold value analysis of YBCO tapes under transient DC over-current impulse. *Phys. C Supercond. Its Appl.* **2018**, *554*, 32–37. [CrossRef]
37. Sheng, J.; Zeng, W.; Yao, Z.; Zhao, A.; Hu, D.; Hong, Z. Recovery time of high temperature superconducting tapes exposed in liquid nitrogen. *Phys. C Supercond. Its Appl.* **2016**, *527*, 50–54. [CrossRef]
38. Maeda, C.; Yanai, S.; Shirai, Y.; Shiotsu, M.; Honda, G.; Isojima, S. Recovery characteristics of GdBCO tape in a pressurized liquid nitrogen for a resistive SFCL. *IEEE Trans. Appl. Supercond.* **2019**, *29*, 5602505. [CrossRef]
39. Xiang, B.; Gao, L.; Junaid, M.; Liu, Z.; Geng, Y.; Wang, J.; Yanabu, S. Effects of Magnetic Fields on Quench Characteristics of Superconducting Tape for Superconducting Fault Current Limiter. *Appl. Sci.* **2019**, *9*, 1466. [CrossRef]
40. Rusiński, J.; Hajdasz, S.; Kempski, A. Analysis of recovery time under load conditions and energy dissipation of superconducting tapes with electrical insulation for SFCL applications. In Proceedings of the 2019 Progress in Applied Electrical Engineering, Koscielisko, Poland, 17–21 June 2019.

41. Jiang, Z.; Wang, Y.; Dai, S.; Ma, T.; Peng, C.; Liu, M.; Chen, H. Influence of Insulation on Quench and Recovery of YBCO Tape Under DC Impact. *IEEE Trans. Appl. Supercond.* **2018**, *29*, 7700305. [CrossRef]
42. Liang, S.; Tang, Y.; Ren, L.; Xu, Y.; Wang, W.; Hu, Z.; Zhang, B.; Jiao, F. A novel simplified modeling method based on R–Q curve of resistive type SFCL in power systems. *Phys. C Supercond. Its Appl.* **2019**, *563*, 82–87. [CrossRef]
43. Liang, S.; Ren, L.; Ma, T.; Xu, Y.; Tang, Y.; Tan, X.; Li, Z.; Chen, G.; Yan, S.; Cao, Z.; et al. Study on quenching characteristics and resistance equivalent estimation method of second-generation high temperature superconducting tape under different overcurrent. *Materials* **2019**, *12*, 2374. [CrossRef] [PubMed]
44. Lv, Y.; Jiang, J.; Yao, L.; Ryu, K.; Li, Z.; Hong, Z.; Jin, Z. Experimental results of various optical fibers encapsulated HTS tapes under impulse currents for the SFCL application. *IEEE Trans. Appl. Supercond.* **2020**, *30*, 9001605. [CrossRef]